THE JOURNAL OF PHYSICAL CHEMISTRY C

ARTICLE

pubs.acs.org/JPCC

Anisotropic Lithium Insertion Behavior in Silicon Nanowires: Binding Energy, Diffusion Barrier, and Strain Effect

Qianfan Zhang,[†] Yi Cui,[*,‡] and Enge Wang[†,§]

[†]Institute of Physics, Chinese Academy of Sciences, Beijing 100190, China

[‡]Department of Materials Science and Engineering, Stanford University, Stanford, California 94305, United States

[§]School of Physics, Peking University, Beijing 100871, China

ABSTRACT: Silicon nanowires (SiNWs) have recently been shown to be promising as high capacity lithium battery anodes. SiNWs can be grown with their long axis along several different crystallographic directions. Due to distinct atomic configuration and electronic structure of SiNWs with different axial orientations, their lithium insertion behavior could be different. This paper focuses on the characteristics of single Li defects, including binding energy, diffusion barriers, and dependence on uniaxial strain in [110], [100], [111], and [112] SiNWs. Our systematic ab initio study suggests that the Si−Li interaction is weaker when the Si−Li bond direction is aligned close to the SiNW long axis. This results in the [110] and [111] SiNWs having the highest and lowest Li binding energy, respectively, and it makes the diffusion barrier along the SiNW axis lower than other pathways. Under external strain, it was found that [110] and [001] SiNWs are the most and least sensitive, respectively. For diffusion along the axial direction, the barrier increases (decreases) under tension (compression). This feature results in a considerable difference in the magnitude of the energy barrier along different diffusion pathways.

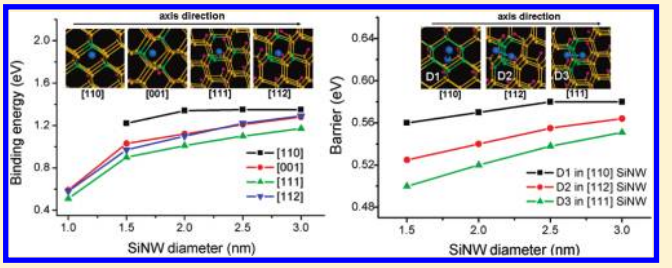

INTRODUCTION

Recently, silicon nanowires (SiNWs) have been demonstrated as ultrahigh capacity lithium ion battery negative electrodes;[1] this opens up exciting opportunities for energy storage devices. Silicon has the highest known specific charge capacity (4200 mAh/g); this value is ∼10 times greater than that of the graphitic carbon used in existing technology.[2] However, in bulk Si, Li insertion causes a volume expansion up to four times the original volume, which induces structural changes and mechanical fracture of Si. SiNWs and other Si nanostructures[3−7] have been shown to overcome the fracture issues and to perform well as anodes due to their strain relaxation capability.[1] Furthermore, SiNWs possess excellent properties for Li insertion, such as efficient electron transport along the axis and large Li ion flux due to the high surface area to volume ratio. SiNWs are known to have different crystallographic orientations and can be fabricated with different diameters.[8,9] However, experimental investigations have not paid much attention to Li insertion behavior in SiNWs with different orientations and different sizes, especially when the Li doping ratio is very low and the SiNW is ultrathin. These features are very important in revealing the nature of quantum confinement effects and the fundamental mechanics of Li insertion and diffusion. Although some theoretical works have focused on the Li−SiNW interaction,[10] the effect of anisotropy on the interaction of Li with SiNWs of different orientations still remains unclear.

One of the most important anisotropic effects in the confined system relates to the response to external strain. Imposing strain is a common way to change the properties of material and improve device performance. SiNW strain studies, both experimental and theoretical, have shown remarkable changes in NW properties, like great enhancement of carrier mobility[11,12] and significant modification of band structure,[13,14] especially when the diameter is small. Recently, a theoretical study indicated that a strained SiNW can open up a new avenue for application in solar cells.[15] Therefore, it can be predicted that the strain can also affect the Li insertion in SiNWs for energy storage application. Furthermore, strain exists naturally in real SiNWs, and its occurrence is almost unavoidable during the growth process. Therefore, the theoretical simulation of Li insertion in strained SiNWs is also helpful to assist in experimental understanding.

We have previously studied general properties of single Li insertion in SiNWs,[16] but we have not yet focused on orientation-dependent properties. In this work, we study systematically the relationship between Li insertion behavior and SiNW orientation. We performed first-principle simulations on [110], [100], [111], and [112] SiNWs with single Li impurities with and without strain. It was found that the Si−Li interaction becomes weaker as the Si−Li bond inclines toward the SiNW axis

Received: December 6, 2010
Revised: February 28, 2011

dx.doi.org/10.1021/jp1115977 | J. Phys. Chem. C XXXX, XXX, 000–000

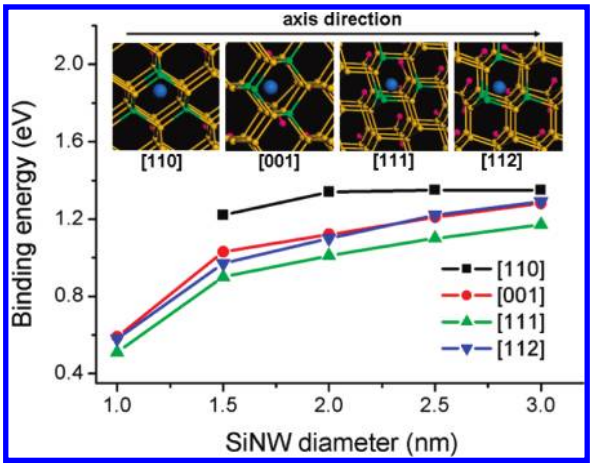

Figure 1. Li binding energy E_b in [110], [001], [111], and [112] SiNWs with diameters of $d \approx 1.0$, 1.5, 2.0, and 2.5 nm. The insets show the side view of these SiNWs (axis direction is along the x-axis) and the stable insertion site for a Li impurity. The large blue sphere represents the Li impurity, and the green spheres represent the four neighboring Si atoms.

direction. Due to this effect, the [110] SiNWs and [111] SiNWs have the highest and lowest binding energy, respectively, and the diffusion barrier decreases when the diffusion direction is inclined close to the SiNW axis. Through the study of the uniaxial strain effect, we found that [110] and [001] SiNWs are the most and least sensitive to external strain with respect to changes in Li binding energy, respectively. When the Li diffusion direction is close to the axial direction, the barrier will decrease (increase) under compression (tensile), while the diffusion barrier follows the opposite behavior when the diffusion pathway is along the SiNW cross-sectional plane.

COMPUTATIONAL METHOD

First-principle calculations were performed using the Vienna ab initio simulation program (VASP) in the framework of density functional theory (DFT).[17,18] We have proven that Li insertion or diffusion in core sites can be treated as representative of Li insertion behavior;[16] therefore, our study concentrates on Li insertion and diffusion in the core region near the center of the NW. Si atoms on the surface are passivated by H atoms to make sure that all the Si atoms have a coordination number of four and that no dangling Si bonds exist. The vacuum between a SiNW and its image exceeds 18 Å, while the distance between an inserted Li atom and its image is no less than 11 Å along the axial direction. Such a system is large enough to avoid any artificial interaction between images after our careful tests. The PAW pseudopotential[19] was adapted, and the GGA exchange-correlation function was described by Perdew and Wang (PW91).[20] $1 \times 1 \times 3$ Monkhorst–Pack k-point meshes[21] were used, and the plane-wave basis set shares the same energy cutoff of 400 eV. The structural relaxation was performed using the conjugate gradient minimization method to ensure that the force on each atom is less than 0.02 eV/Å. To calculate the Li diffusion barrier in SiNWs, we used the nudged elastic band scheme.[22]

ANISOTROPIC EFFECT IN UNSTRAINED SINWS

First, we studied the Li binding energy E_b on near-center insertion positions in four types of SiNWs. It has been demonstrated that the stable site for the Li defect is a tetrahedral (Td) interstitial site with four nearest Si atoms, both in SiNWs and in bulk Si.[16,23] E_b is defined as the energy difference between the Li-inserted SiNW system (E_{tot}) and the summation of a single Li atom (μ_{Li}) and a pristine SiNW (E_{SiNW})

$$E_b = E_{SiNW} + \mu_{Li} - E_{tot}$$

A larger E_b denotes more stable Li–Si binding. The E_b values for four types of SiNWs with diameters of $d \approx 1.0$, 1.5, 2.0, and 2.5 nm are shown in Figure 1. For all the SiNWs, the binding energy increases as the diameter grows. The series of [110] SiNWs has the highest binding energy, while the [111] SiNWs have the lowest, which indicates that they are the least and most sensitive to quantum confinement effects, respectively. The series of [001] and [112] SiNWs have similar intermediate E_b values.

To clarify this anisotropic effect in different types of SiNWs, we focus our study on the Si–Li bonds perpendicular (or vertical) and parallel (lateral) to the SiNW long axis, which are marked as V-Bond and L-Bond, respectively. The former exists in [110] SiNWs, while the latter exists in [111] SiNWs. We calculated the charge density difference $\Delta\rho$ along both types of Si–Li bonds in SiNWs with different diameters. $\Delta\rho$ is expressed as

$$\Delta\rho = \rho[\mathrm{Li/SiNW}] - \rho[\mathrm{Li}] - \rho[\mathrm{SiNW}]$$

which represents the electron drift when placing a Li impurity in a SiNW. The illustrations of the V-Bond and L-Bond and their $\Delta\rho$ curves are shown as Figure 2. It can be clearly seen that the L-Bond is more sensitive to diameter than the V-Bond. For the L-Bond, charge transfer along the Si–Li line increases as the SiNW diameter increases, which means there is a stronger interaction between the Li defect and a neighboring Si atom. However, the V-bond is nearly independent of the diameter of the SiNW. Therefore, it can be concluded that the quantum effect has a large influence on the Si–Li bonds along the SiNW long axis but has little effect on the vertical Si–Li bonds. This observation can explain why different SiNW orientations lead to the different E_b values shown in Figure 1. In [110] SiNWs, two V-bonds exist which are not sensitive to quantum confinement, while in [111] SiNWs, the L-Bond is dramatically affected by quantum confinement. Such bond orientation anisotropy leads to the highest and lowest Li binding energy in the series of [110] and [111] SiNWs, respectively. The Li–Si bonds in [001] and [112] SiNWs are all angled (A-Bond), and the strength of these Si–Li bonds falls in between that of the V-Bond and L-Bond.

This anisotropic bonding effect also exerts an influence on the Li diffusion barriers along different directions. In Figure 3, the barrier heights for [110], [111], and [112] SiNWs are plotted versus diameter; the diffusion paths are indicated by D-1, D-2, and D-3, respectively. The Li diffusion pathway between two Td sites is approximately a straight line, and the three pathways are at angles of 90°, 13°, and 0° to the SiNW axis, respectively. It is evident that the D-1 barrier shows little change with diameter, but the D-2 and D-3 barrier heights increase with diameter and approach the bulk value of 0.58 eV when the SiNW diameter is greater than 3 nm. In 1.5 nm [111] SiNWs, the D-3 diffusion barrier is 75 meV smaller than the bulk, which is significant enough to cause a performance difference in Li ion battery operation.

dx.doi.org/10.1021/jp1115977 |J. Phys. Chem. C XXXX, XXX, 000–000

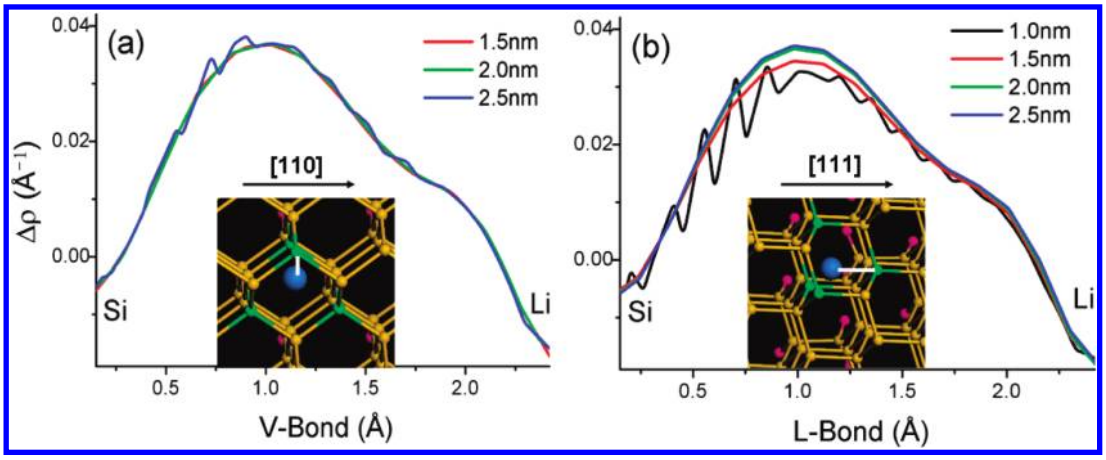

Figure 2. Charge density difference $\Delta\rho$ along the Si−Li bond. (a) and (b) represent a V-Bond in the series of [110] SiNWs and an L-Bond in the series of [111] SiNWs, respectively. The white lines in the insets illustrate two kinds of Si−Li bonds.

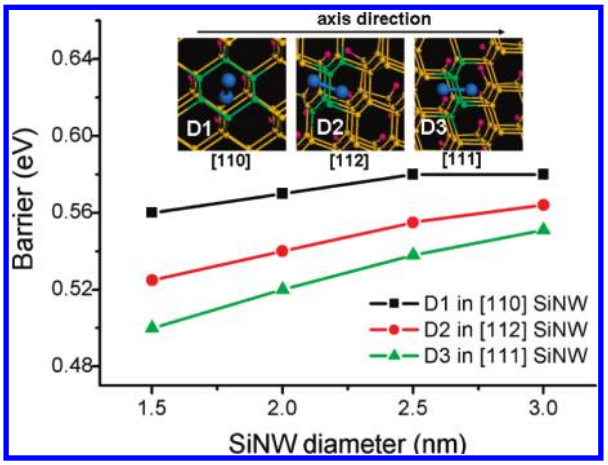

Figure 3. Barriers for D1, D2, and D3 diffusion processes in [110], [112], and [111] SiNWs with different diameters. The insets illustrate D1, D2, and D3 diffusion processes using blue lines, which occur in [110], [001], and [111] SiNWs, respectively. The small green spheres are the six Si neighbors of the Li impurity on the Hex site.

The transition state for Li diffusion is the hexagonal (Hex) site.[16] When located on a Hex site, a Li defect has six Si neighbors, and their configuration can be viewed as two parallel triangles, both of which are perpendicular to the diffusion pathway. As in the Td site case, the strength of the interaction between a Hex-sited Li defect and its Si neighbors follows similar Si−Li bond direction dependence; the Si−Li bond becomes stronger as the triangles become parallel to the cross plane of the SiNW because of the nearly vertical-axis Si−Li bonds. In most diffusion processes, Td-sited and Hex-sited Li defects have similar Si−Li bond directions, such as the D-1 pathway, during which Li defects have two V-Bonds and two A-bonds on the Td site and two V-bonds and four A-bonds on the Hex site. As a result, this anisotropic effect on Td-sited and Hex-sited Li defects almost cancels, which induces a similar barrier to that in bulk Si. However, for lateral-axis diffusion, such as the D-3 process, the Hex Si triangles are perpendicular to the axial direction, which results in the most stable Hex energy. At the same time, the L-Bond on the Td site induces the least stable Td-sited energy. Therefore, the combination of these two features causes the diffusion barrier along or near to the axial direction to be lower than that of angled diffusion.

STRAIN EFFECT IN DIFFERENT ORIENTATED SINWS

Next, we studied Li insertion behavior when external uniaxial strain is applied to SiNWs. In experiment, such strain can be obtained by a process involving embedded SiGe or a capping layer (such as deposition of intrinsic SiO_2 or Si_3N_4).[24,25] To theoretically simulate the strained Li−SiNW system, the length of the z-axis vector was fixed at a specified value and forbidden to change during structural relaxation. The axial length change percentage $\varepsilon = (L - L_0)/L_0$ (L and L_0 represent z-axis vector length with and without strain) is used as the parameter to measure the extent of strain, and positive (negative) ε means that tensile (compressive) strain is applied. We calculated the center-Td-sited Li binding energy change $\Delta E_b(\varepsilon) = E_b(\varepsilon) - E_b(0)$ in 1.5 nm diameter [110], [001], [111], and [112] SiNWs with strain values ranging from $\varepsilon = -5\%$ to $\varepsilon = 5\%$, and the result is shown in Figure 4(a). The Li binding energy in the [110] SiNW is the most sensitive to strain; the binding energy depends nearly linearly on strain. The strain effect is smaller in other types of SiNWs, and the [001] SiNWs show the least dependence. At $\varepsilon = 5\%$, we calculated ΔE_b values in all types of SiNWs with diameters of $d \approx 1.5$, 2.0, 2.5, and 3.0 nm. The ΔE_b versus d curves, as shown in Figure 4(b), are flat, which indicates that ΔE_b depends weakly on the SiNW size.

In our previous study, we showed that the Si equilibrium lattice spacing is small for accommodation of a Li atom.[16,23] If the SiNW stretches, the volume of the lattice expands, and the Li impurity has more space to be accommodated. At $\varepsilon = 5\%$, we computed the length changes of differently oriented Si−Si bonds in undoped SiNWs and differently oriented Si−Li bonds in Li-doped SiNWs, which are measured by $bl_{Si-Si} = \Delta d_{Si-Si}/d_{Si-Si}$ and $bl_{Si-Li} = \Delta d_{Si-Li}/d_{Si-Li}$, respectively ($d_{x-x}$ represents the x−x bond length in an unstrained SiNW, and Δd_{x-x} represents the x−x bond length change under strain). Illustrations of these Si−Si bonds (SS1−SS4) and Si−Li bonds (SL1−SL4) and their length changes are shown as Figure 4(c) and (d), respectively. Under tensile strain, both Si−Si bonds and Si−Li bonds expand, and the elongation increases as the bond

dx.doi.org/10.1021/jp1115977 |J. Phys. Chem. C XXXX, XXX, 000–000

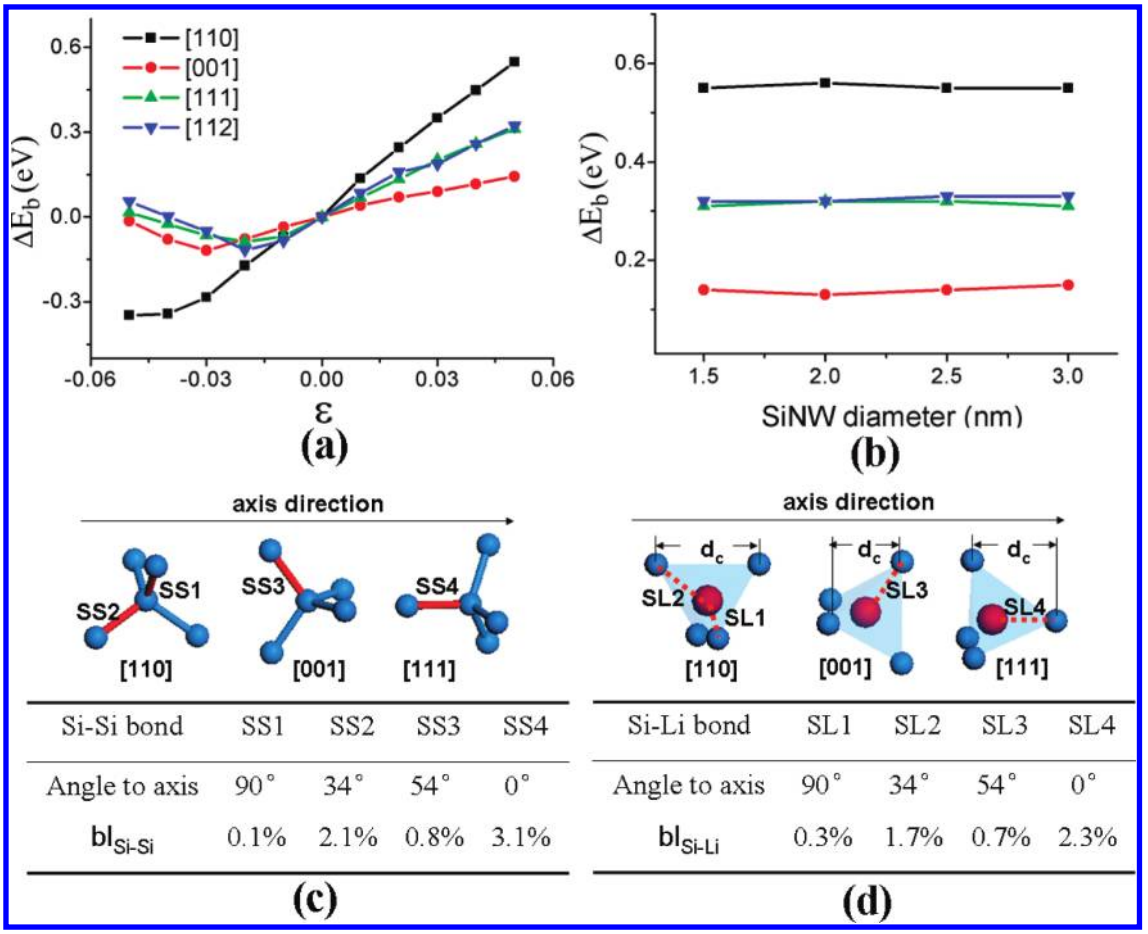

Si-Si bond	SS1	SS2	SS3	SS4
Angle to axis	90°	34°	54°	0°
bl_{Si-Si}	0.1%	2.1%	0.8%	3.1%

Si-Li bond	SL1	SL2	SL3	SL4
Angle to axis	90°	34°	54°	0°
bl_{Si-Li}	0.3%	1.7%	0.7%	2.3%

Figure 4. (a) Binding energy change ΔE_b in 1.5 nm [110], [001], [111], and [112] SiNWs at $\varepsilon = -5\%$. (b) ΔE_b in four types of SiNWs with diameters $d \approx 1.5$ and -3.0 nm at $\varepsilon = 5\%$. (c) The insets show four typical Si−Si bonds, denoted SS1, SS2, SS3, and SS4, which are marked by red lines in [110], [001], and [111] SiNWs. The table lists these bonds' angles to the axis and their elongation parameter bl_{Si-Si} at $\varepsilon = 5\%$. (d) The insets show four typical Si−Li bonds, named SL1, SL2, SL3, and SL4, which are marked by dashed red lines in [110], [001], and [111] SiNWs. The table lists these bonds' angles to the axis and their elongation parameter bl_{Si-Li} at $\varepsilon = 5\%$.

orientation approaches the SiNW axial direction. This is the reason why [110] SiNWs, which have two SS2 bonds nearly along the SiNW axis, have the largest ΔE_b (Figure 4(a)) and [001] SiNWs, which have four inclined SS3 bonds, have the smallest ΔE_b. Such strain dependence can be understood because when uniaxial strain is applied the Si lattice structure in the axial direction changes greatly, but the shape in the cross plane remains relatively unchanged as a result of the low Poisson ratio (the parameter that gives the ratio between diameter change and axial length change).[15] On the basis of this behavior, we can also intuitively estimate such a strain effect by considering the characteristic length d_c, which can be viewed as the projected length of a Si tetrahedron on the axial direction, as marked in Figure 4(d). The sensitivity of the ΔE_b dependence on strain is proportional to d_c. In [110] SiNWs, d_c equals the side length of the tetrahedron, while in [001] SiNWs, d_c equals the length of the midpoint-connected line between two opposite sides; these are the longest and shortest d_c values among all possible projected lengths of the tetrahedron, respectively.

Finally, we studied the core-region diffusion barrier $V(\varepsilon)$ in four types of 1.5 nm SiNWs when $\varepsilon = -5\%$, 0%, and 5%, which serve as representative compressed, unstrained, and stretched states in the SiNWs. The barriers of typical diffusion processes are calculated, and the illustrations of these processes are shown as Figure 5. There are two nonequivalent pathways in [110], [001], and [111] SiNWs, while there are three nonequivalent pathways in [112] SiNWs. These results clearly indicate strong barrier dependence on diffusion direction, and the tendency of barrier variance under strain greatly changes as the diffusion pathway grows parallel to axis. Under tensile (compression), the 1 → 2 process in [110] or [112] SiNWs, which is perpendicular to the axis, leads to the largest barrier reduction (increase) among all the processes. The 1 → 3 process in a [110] strained SiNW, for which the axial angle is 35°, has a similar barrier height as an unstrained wire; when the angle between the diffusion pathway and the axis is very small, like in the 1 → 3 process in [111] or [112] SiNWs, the barrier becomes larger (smaller) than the unstrained case. Such a dependence of the barrier on diffusion direction is caused by different energy changes between the Td and Hex site. In a common case, under tensile strain, the Hex-sited Li impurity will gain more energy compared with the Td-sited Li impurity due to more Si neighbors, which induces barrier reduction. However, as the diffusion pathway becomes parallel to the axis, the Si-neighbor triangles for a Hex-sited Li impurity trend parallel to the SiNW cross-sectional plane, and the strain

dx.doi.org/10.1021/jp1115977 |J. Phys. Chem. C XXXX, XXX, 000–000

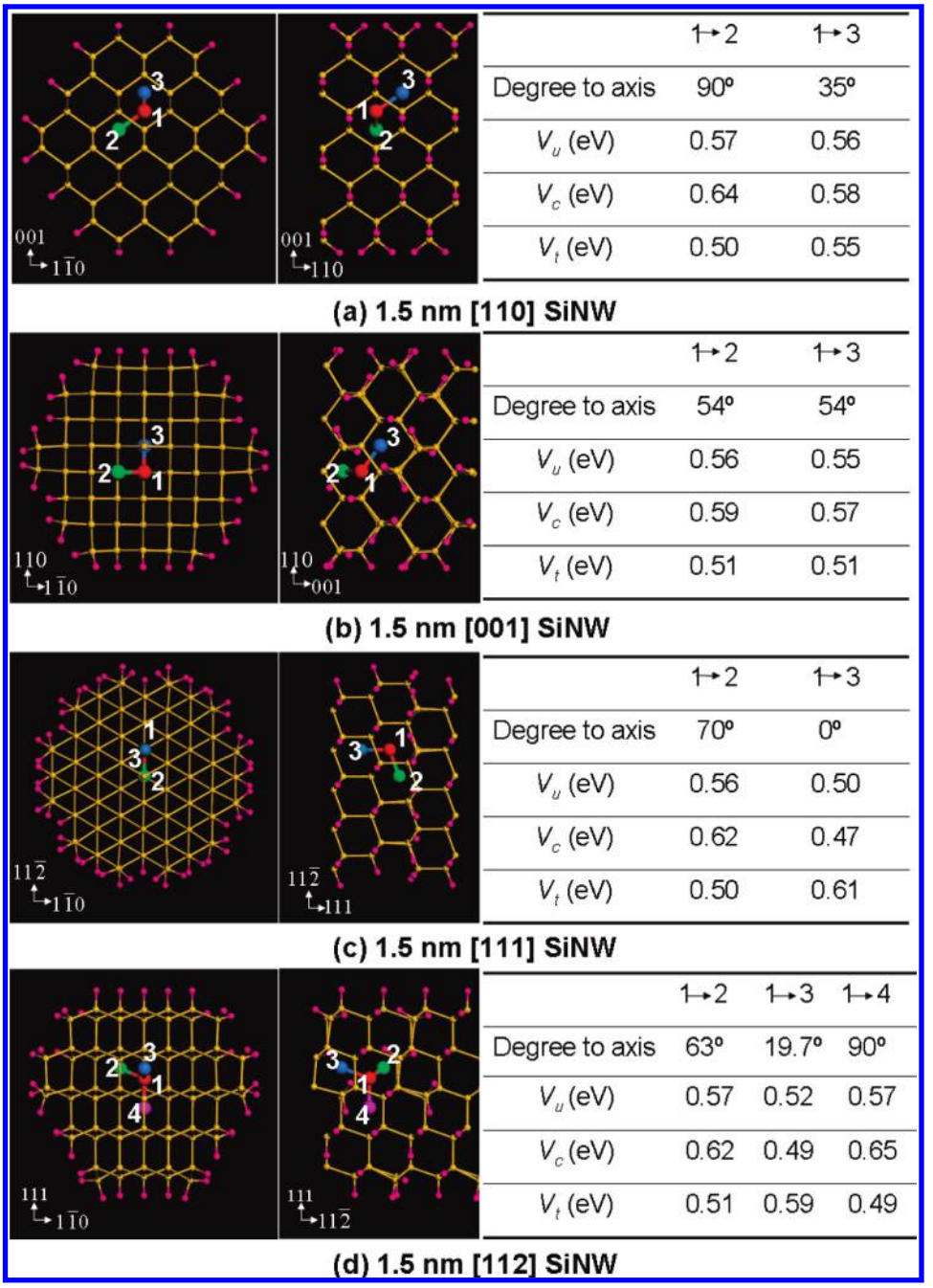

	1→2	1→3
Degree to axis	90°	35°
V_u (eV)	0.57	0.56
V_c (eV)	0.64	0.58
V_t (eV)	0.50	0.55

	1→2	1→3
Degree to axis	54°	54°
V_u (eV)	0.56	0.55
V_c (eV)	0.59	0.57
V_t (eV)	0.51	0.51

	1→2	1→3
Degree to axis	70°	0°
V_u (eV)	0.56	0.50
V_c (eV)	0.62	0.47
V_t (eV)	0.50	0.61

	1→2	1→3	1→4
Degree to axis	63°	19.7°	90°
V_u (eV)	0.57	0.52	0.57
V_c (eV)	0.62	0.49	0.65
V_t (eV)	0.51	0.59	0.49

Figure 5. Illustration of typical Li diffusion processes in 1.5 nm SiNWs with axial directions along (a) [110], (b) [001], (c) [111], and (d) [112] and their barrier values when $\varepsilon = -5\%$ (V_c), 0% (V_u), and 5% (V_t).

influence vanishes because their configurations vary weakly. Therefore, the Td-sited energy decrease causes a higher barrier. Under compression, the barrier change is the opposite. To study the dependence of the strain effect on SiNW size, we calculated the barrier change, defined as $\Delta V(\varepsilon) = V(\varepsilon) - V(0)$ for $\varepsilon = 5\%$, for the $1 \rightarrow 2$ process for the series of [110] SiNWs and the $1 \rightarrow 3$ process for the series of [001] SiNWs and [111] SiNWs with diameters of $d \approx 1.5$, 2.0, 2.5, and 3.0 nm. The dependence of ΔV on diameter is shown in Figure 6. It can be clearly seen that the barrier height in strained SiNWs depends very little on diameter.

Li impurities prefer to follow low-barrier diffusion pathways. For unstrained SiNWs, the barrier height difference among various diffusion directions is small (Figure 5). However, our results show that the barriers are orientation-dependent in strained SiNWs. For [001] SiNWs, all Li diffusion pathways have inclined angles similar to the SiNW axis, so all the barriers will change uniformly. However, for other types of strained SiNWs, the barrier can be quite different in different diffusion directions, and the Li defect prefers to diffuse radially (axially) under tensile (compression), especially for [111] and [112] SiNWs. This distinction may result in unbalanced diffusion or Li distribution. Due to weak size dependence, this anisotropy feature can also be observed in SiNWs with larger diameters, which are easy to prepare in practice.

dx.doi.org/10.1021/jp1115977 |J. Phys. Chem. C XXXX, XXX, 000–000

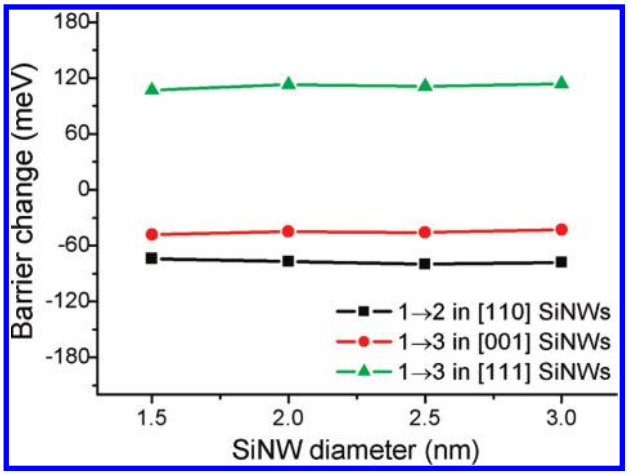

Figure 6. Barrier change $\Delta V(\varepsilon) = V(\varepsilon) - V(0)$ for the $1 \rightarrow 2$ process in [110] SiNWs, the $1 \rightarrow 3$ process in [001] SiNWs, and the $1 \rightarrow 3$ process in [111] SiNWs when $\varepsilon = 5\%$.

SUMMARY

In conclusion, we have studied anisotropic Li insertion behavior, including binding energy, diffusion barriers, and strain effects, in different types of SiNWs. Our results show that distinct Li insertion behaviors in various types of SiNWs are caused fundamentally by a Si−Li bond with respect to the SiNW long-axis orientation. In a binding energy study, we found that the [110] SiNWs have the largest Li binding energy and are the most sensitive response to uniaxial strain; while in the diffusion barrier study, the result showed that the behavior of lateral-axis or nearly lateral-axis diffusion differs from other cases, both in strained and unstrained SiNWs. Our ab initio study provides a valuable fundamental understanding of anisotropic Li insertion behaviors in SiNWs and, at the same time, suggests promising routes for future electrochemical applications.

ACKNOWLEDGMENT

This work was supported by CAS and NSFC. E.W. acknowledges Stanford's GCEP visiting scholar program. We also gratefully acknowledge the computational time provided by the Swedish agency SNAC. Y.C. acknowledges support from the King Abdullah University of Science and Technology (KAUST) Investigator Award (No. KUS-l1-001-12), Stanford GCEP, and US ONR.

REFERENCES

(1) Chan, C.; Peng, H.; Liu, G.; McIlwrath, K.; Zhang, X. F.; Huggins, R. A.; Cui, Y. *Nat. Nanotechnol.* **2008**, *3*, 31.
(2) Boukamp, B.; Lesh, G.; Huggins, R. *J. Electrochem. Soc.* **1981**, *128*, 725.
(3) Cui, L. F.; Ruffo, R.; Chan, C. K.; Peng, H.; Cui, Y. *Nano Lett.* **2009**, *9*, 491.
(4) Cui, L. F.; Yang, Y.; Hsu, C. M.; Cui, Y. *Nano Lett.* **2009**, *9*, 3370.
(5) Park, M. H.; Kim, M. G.; Joo, J.; Kim, K.; Kim, J.; Ahn, S.; Cui, Y.; Cho, J. *Nano Lett.* **2009**, *9*, 3844.
(6) Kim, H.; Han, B.; Choo, J.; Cho, J. *Angew. Chem.* **2008**, *47*, 10151.
(7) Esmanski, A.; Ozin, G. A. *Adv. Funct. Mater.* **2009**, *19*, 1999.
(8) Wu, Y; Cui, Y.; Huynh, L.; Barrelet, C. J.; Bell, D. C.; Lieber, C. M. *Nano Lett.* **2004**, *4*, 433.
(9) Cui, Y.; Lauhon, L. J.; Gudiksen, M. S.; Wang, J. F.; Lieber, C. M. *Appl. Phys. Lett.* **2001**, *78*, 2214.
(10) Chan, T. L.; Chelikowsky, J. R. *Nano Lett.* **2010**, *10*, 821.
(11) Leong, M.; Doris, B.; Kedzierski, J.; Rim, K.; Yang, M. *Science* **2004**, *306*, 2057.
(12) Liu, C. W.; Maikap, S.; Yu, C.-Y. *IEEE Circuits Devices Mag.* **2005**, *21*, 21.
(13) Hong, K.-H.; Kim, J.; Lee, S.-H.; Shin, J. K. *Nano Lett.* **2008**, *8*, 1335.
(14) Leu, P. W.; Svizhenko, A; Cho, K. *Phys. Rev. B* **2008**, *77*, 235305.
(15) Wu, Z. G; Neaton, J. B.; Grossman, J. G. *Nano Lett.* **2009**, *9*, 2418.
(16) Zhang, Q. F.; Zhang, W. X.; Wan, W. H.; Cui, Y.; Wang, E. G. *Nano Lett.* **2010**, *10*, 3243.
(17) Kresse, G.; Hafner, J. *Phys. Rev. B* **1993**, *48*, 13115.
(18) Kresse, G.; Furthmuller, J. *Phys. Rev. B* **1996**, *54*, 11169.
(19) Blochl, P *Phys. Rev. B* **1994**, *50*, 17953.
(20) Wang, Y.; Perdew, J. *Phys. Rev. B* **1991**, *44*, 13298.
(21) Monkhorst, H. J.; Pack, J. D. *Phys. Rev. B* **1976**, *13*, 5188.
(22) Jonsson, H.; Mill, G.; Jacobsen, K. W. In *Classical and Quantum Dynamics in Condensed Phase Simulations*; Berne, B. J., Ciccotti, G., Coker, D. F., Eds.; World Scientific: Singapore, 1998.
(23) Wan, W. H.; Zhang, Q. F.; Cui, Y.; Wang, E. G. *J. Phys.: Condens. Matter* **2010**, *22*, 415501.
(24) Trinkaus, H.; Holländer, B.; Mantl, S; Herzog, H. −J; Kuchenbecker, J.; Hackbarth, T. *Appl. Phys. Lett.* **2000**, *76*, 3552.
(25) Buca, D.; Holländer, B.; Feste, S.; Lenk, St.; Trinkaus, H.; Mantl, S. *Appl. Phys. Lett.* **2007**, *90*, 32108.

dx.doi.org/10.1021/jp1115977 |*J. Phys. Chem. C* XXXX, XXX, 000–000